Study of the $\alpha + \alpha$ system below 15 MeV (c.m.)*

W. S. Chien† and Ronald E. Brown

John H. Williams Laboratory of Nuclear Physics, University of Minnesota, Minneapolis, Minnesota 55455

(Received 12 August 1974)

Differential cross sections for $\alpha + \alpha$ elastic scattering have been measured at lab energies of 18.00, 21.12, 24.11, 25.50, 26.99, 28.50, and 29.50 MeV. The majority of the data have relative errors less than 1%, and the additional error in absolute scale is 0.30%. A phase-shift analysis of the data has been performed, and most of the phase shifts have been determined to within $\pm\frac{1}{3}°$. These phase shifts and others from the literature were used to study properties of the $\alpha + \alpha$ system in the center of mass energy range 1.50 to 14.74 MeV. First, an R-matrix analysis was made of the $l = 4$ phase shifts; this analysis yields a resonance energy of 11.7 ± 0.4 MeV and a level width at resonance of 4.0 ± 0.4 MeV. Second, comparison was made of the $\alpha + \alpha$ phase shifts with results of previous resonating-group calculations, and this comparison shows good agreement with a calculation which includes one inelastic channel and a nucleon-nucleon repulsive core. Third, an $\alpha + \alpha$ potential model was constructed. This model contains an attractive potential obtained by folding Gaussian α-particle densities together with a Yukawa-shaped direct part of a nucleon-nucleon potential and, in addition, contains phenomenological short-range repulsive components in the $l = 0$ and $l = 2$ states. The model reproduces the experimental phase shifts quite well when the Yukawa potential is taken to have a range corresponding to a two-pion mass.

I. INTRODUCTION

The fundamental importance to nuclear physics of the interaction between two α particles has long been recognized, and consequently, this interaction has been the subject of much theoretical[1-12] and experimental[13-19] study. The spin-isospin saturation and high binding energy of the α particle suggest that α-particle-like substructures might be important constituents of light nuclei[20] or of the surface region of heavy nuclei.[21] Therefore, a detailed knowledge of the $\alpha + \alpha$ interaction possibly could clarify certain aspects of nuclear reaction mechanisms and nuclear structure. In particular, recent α-particle-model calculations[22] of properties of ^{12}C and ^{16}O have shown the usefulness of a description of the $\alpha + \alpha$ interaction in terms of a phenomenological potential.[3,19] The $\alpha + \alpha$ system is also a very important one for the testing of calculations using the resonating-group[23] method, which has been quite successful in describing interactions between very light nuclei. This importance rests in the fact that the α particle is such that many of the approximations of the resonating-group method are expected to be quite valid for the $\alpha + \alpha$ system, especially at center of mass (c.m.) energies below the reaction threshold of 17.35 MeV. Thus, it is of considerable interest to compare such calculations with precise ex-

perimental results in this low-energy region. An additional important aspect of the $\alpha + \alpha$ interaction arises from some of its theoretically deduced characteristics.[1,2,10] These are that exchange effects, such as those caused by the Pauli exclusion principle, can be represented by an l-dependent repulsive potential of short range and that the long-range part of the interaction can be represented by an attractive potential to which only the direct part of the nucleon-nucleon potential makes a significant contribution.[24] Consequently, it has been proposed[3] that an accurate determination of the long-range part of the $\alpha + \alpha$ potential may provide information on the direct component of the nucleon-nucleon force.

In the present work we have measured differential cross sections for $\alpha + \alpha$ elastic scattering at seven bombarding energies between 18 and 30 MeV, and have expended substantial effort to make these measurements in an accurate manner. The majority of the data have relative standard deviations of less than 1%, and the standard deviation in the absolute scale is 0.30%. The methods used in carrying out the experiment and in reducing the data to differential cross sections are discussed in Secs. II and III. The extraction of phase shifts from the cross-section values is described in Sec. IV. Most of the phase shifts have been determined to within $\frac{1}{3}°$, which is an accuracy con-

siderably greater than that reported previously[14-16] in energy ranges which overlap that of the present experiment. In Sec. V we relate how our phase shifts and others[15-18] from the literature have been used to study properties of the $\alpha + \alpha$ system in the c.m. energy range 1.50 to 14.74 MeV. In that section we describe an R-matrix analysis of the $l = 4$ phase shift, a comparison of the $\alpha + \alpha$ phase shifts with those obtained from current resonating-group calculations, and a potential-model analysis of the phase shifts. In the latter analysis, emphasis is given to obtaining a description of the long-range part of the $\alpha + \alpha$ interaction with a view toward probing the direct part of the nucleon-nucleon interaction. Finally, concluding remarks are made in Sec. VI.

II. EXPERIMENT

A. Apparatus

The MP tandem Van de Graaff accelerator at the Williams Laboratory was used to produce α-particle beams of the desired energies. The energy of the particle beam is determined by the require-ment that the beam undergo a 90° deflection in a calibrated analyzing magnet. The original calibra-tion[25] of this magnet was accurate to about $\pm 0.04\%$, which yields an uncertainty of about ± 10 keV in the α-particle bombarding energies used here. Soon after the present experiment was completed, the magnet calibration was rechecked[26] by an observa-tion of the well known[27] $T = \frac{3}{2}$ resonance in $^{12}C(p,p)$ near 14-MeV proton bombarding energy. The resonance energy obtained using the original cali-bration constant of the analyzing magnet was 4 keV different from the accepted value.[28] This difference is not significant in the present experi-ment, because of the uncertainties arising from corrections for energy loss in the gas cell.

The scattering chamber[29] is of 43-cm diameter and contains independently rotatable, radially grooved upper and lower turntables. Before data taking was begun, a thorough chamber alignment was carried out and tests for reproducibility of the turntable angular settings were made.[30] This procedure involved the use of a precision align-ment telescope[31] having integrated micrometers, which allow direct measurement of object vertical and horizontal displacements from the optical axis. The alignment of the data-detector collimator assembly, which was mounted in one of the grooves of the lower turntable, was also checked during chamber alignment. It was determined that the angle at which the symmetry axis of the detector collimator assembly intersects the optically defined beam line in known to $\pm 0.03°$ and is repro-ducible to one-half of this value.

Two detector assemblies were used. One served as a monitor at a fixed angle and the other served to measure differential cross sections. This latter assembly (the data-detector assembly) consisted of a parallel-edged front aperture, a rectangular rear aperture, and intermediate antiscattering baffles, all mounted in a tube of 1.9-cm i.d. and all carefully fabricated from 250-μm-thick tantalum sheet. The approximate dimensions of the data-detector assembly were: width $2a$ of front aperture $= 1$ mm, width $2b$ of rear aperture $= 1$ mm, height l of rear aperture $= 5$ mm, distance h between front and rear apertures $= 140$ mm, and distance R_0 of the rear aperture from the scattering-cham-ber center $= 189$ mm. For this assembly the lowest-order geometry factor $G_{00} = 4abl/(hR_0)$, had the approximate value 1.8×10^{-5} cm sr. The important aperture dimensions were measured to accuracies ranging from ± 0.001 to ± 0.002 mm. These measurements were carried out using a 30-power microscope with a micrometer-driven traveling stage,[32] whose micrometer-dial calibra-tion was checked by measuring the dimensions of several standard blocks.[33] The aperture dimen-sions measured in this way were reproduced by independent measurements on a 20-power shadow-graph. The accuracy with which all relevant dimensions of the data-detector assembly are known results in the value of G_{00} being known to $\pm 0.23\%$. The particle detector was a silicon, surface-barrier type, having a sensitive area of 100 mm^2 and a maximum depletion depth of 700 μm. The detector was mounted directly behind the rear aperture, and the entire assembly was accurately and rigidly positioned in one of the radial grooves of the lower turntable. The moni-tor-detector assembly, which was mounted on the upper turntable, had, at different times, geometry factors G_{00} from 2 to 4 times larger than that of the data-detector assembly.

The ^{4}He target gas[34] was contained in gas cells enclosed by 6-μm-thick Kapton foil.[35] This Kapton plastic foil was used because tests[36] showed that the multiple Coulomb scattering of α particles in it is considerably less than in previously used 2.5-μm-thick Havar[37] metallic foil. Most of the data were obtained using a 2.3-cm-diam cylindrical brass cell having 1-cm-high windows separated by two posts. Some forward-angle data were ob-tained using a 3.8-cm-diam brass cell having a 3.5-cm-long snout, through which the beam passes before entering the central volume of the cell. The cell could be evacuated and filled by means of a gas-transfer system which contains a liquid-nitrogen-trapped mechanical pump, provision for passing the target gas through a liquid-nitrogen trap, and an optional 1-liter gas reservoir. The

gas reservoir was necessary in the present experiment, because Kapton foil is somewhat permeable to helium gas. Thus, at the 400 Torr pressure used in the present experiment, the cell pressure would decrease at a rate of about 6 Torr/hr with the reservoir closed off from the system, whereas the cell pressure remained essentially constant over many hours with the reservoir opened to the system.

The instrumentation for determining the pressure and temperature of the gas cell possessed remote readout capabilities, which allowed continual monitoring of the pressure and temperature values. The pressure readout was provided by an electronic pressure transducer[38] of the diaphragm-capacitance bridge type, used with a precision digital volt meter. In addition, an accurate mechanical pressure gauge[39] was included in the gas-transfer system, which was situated near the scattering chamber. Both pressure instruments were calibrated to within ±0.1% by comparison with a mercurial monometer[40] whose accuracy is one part in 3000. The temperature readout was provided by recording the resistance of a semiconductor thermistor,[41] which was embedded in and in close thermal contact with the brass material of the gas cell. The thermistor was calibrated against a mercurial thermometer[42] which carries an NBS certificate of accuracy. The calibration was reproducible to ±0.3°C.

A 178-cm-long 10-cm-diam Faraday cup, with magnetic electron suppression, is attached to the scattering chamber and collects the beam particles after they have passed through the gas cell. The beam-charge-collection efficiency of the Faraday cup arrangement has been investigated and it has been shown[36] that, with Kapton foils on the gas cell and with the scattering-chamber pressure less than 5×10^{-5} Torr, the following processes have negligible effect on charge collection: escape of secondary electrons from the Faraday cup, entrance into the Faraday cup of electrons expelled from the gas cell by beam particles, ionization of residual gas in the scattering chamber, and multiple Coulomb scattering of beam particles in the gas cell. The total beam charge collected in a data-taking period was measured with a commerical[43] beam-current integrator. This integrator was calibrated in our laboratory[30] to an accuracy of ±0.1%, and our calibration agrees with that specified by the manufacturer.

The electronic instrumentation used was quite standard and consisted of charge-sensitive preamplifiers, linear amplifiers, single-channel pulse-height analyzers, computer-interfaced scalars, an analog-to-digital converter (ADC), and an on-line computer. The pulses from the monitor-detector linear amplifier were connected to a single-channel analyzer, and the analyzer output pulses were scaled. The pulses from the data-detector linear amplifier were connected both to a single-channel analyzer and to the ADC. The output of the single-channel analyzer was scaled and was directed to a gating input of the ADC. A comparison of the number of gate pulses with the number of pulses analyzed by the ADC yielded a factor used to correct the data for the ADC dead time.

B. Procedure

At the beginning of each data-taking period, the stainless-steel tubing and reservoir of the gas-transfer system were heated to promote outgassing. The system was then pumped for many hours before ^{4}He gas was transferred into the cell. The α-particle beam was directed through collimators and into the scattering chamber by means of steering and focusing operations. Beam alignment was facilitated by the observation, through closed-circuit television, of the scintillations produced as the beam passed through a thin quartz disk at the scattering-chamber center. The aligned beam had, at the center of the gas cell, a diameter of 1.6 mm and a half angle of divergence of 5 mrad. This divergence angle was caused almost entirely by multiple Coulomb scattering of the beam in the Kapton foil enclosing the cell.

After it was made certain that all the apparatus was functioning properly, data taking was initiated by checking that several previously measured $\alpha + \alpha$ cross sections could be reproduced. Such tests for reproducibility were made many times throughout the course of the experiment and were made at a variety of angles and at all bombarding energies. To measure the cross section at each lab angle, data runs were always made with the data detector set alternately at equal turntable angles to the left and to the right of the incident beam, and usually at least 25 000 counts were accumulated on each side of the beam. The observed left-right asymmetries in the number of counts often corresponded to an angular asymmetry several times larger than the optically determined angular accuracy of ±0.03°. This indicates that usually the main contribution to the observed asymmetry came from deviations of the actual beam direction from the optically defined beam line. The lab-angle sequence in which data were taken was such that possible equipment malfunctions varying slowly with time could be detected by their causing the differential cross section to deviate from a smooth relation to angle.

At each beam energy, the monitor detector was set at an angle such that its counting rate would

not be very sensitive to minor changes in beam direction. Thus its primary purpose was to monitor target-gas density and beam-current-integration efficiency.

After each data run, the contents of the scalers and the data-detector pulse-height spectrum were stored on magnetic tape for subsequent detailed analysis. Other necessary information was recorded manually. During data collection, preliminary analyses of the data were always carried out as a continual check on the consistency of the measurements.

Other data were also acquired during this experiment. Data runs were taken using an empty cell in order to aid in understanding the nature of the background produced by high-order scattering processes initiated by the interaction of the α-particle beam with the cell foil. In addition, $\alpha + {}^{14}N$ elastic differential cross sections were measured at appropriate angles and bombarding energies, because these data were needed in making small corrections to the $\alpha + \alpha$ cross sections for air contamination present in the gas cell. Finally, as one method of checking the over-all accuracy of the entire data-collection system, $p + p$ elastic differential cross sections were measured for several angles at 9.918 MeV (lab), and the appropriate data of Jarmie et al.[44] were well reproduced.

III. DATA REDUCTION AND ERRORS

Under the assumption that the target gas obeys the perfect-gas law, the lab differential cross section $\sigma_L(\theta_L)$ is given in terms of measured quantities by the formula[45]

$$\sigma_L(\theta_L) = 1.6592 \frac{TzN\sin\theta_L}{bPQG} \text{ mb/sr} , \quad (1)$$

where θ_L is the lab scattering angle, T is the target gas temperature, in K, z is the average charge number per beam particle as collected by the Faraday cup, N is the number of detected particles corrected for detector efficiency, electronic dead time, multiple Coulomb scattering in the target, and slit-edge scattering, P is the partial pressure, in Torr, of the molecular type[46] containing the target nucleus of interest, b is the number of target nuclei per molecule, Q is the total beam charge collected, in μC, and G is the geometry factor,[47-49] in 10^{-5} cm sr, which contains effects of the detection and beam geometries, and, if the variation in cross section with angle is taken into account, G can be used to correct the data for finite angular resolution.

The accuracy with which the quantities T and Q of Eq. (1) and the total pressure were measured has been discussed in Sec. II A, and the errors[50]

for these and other quantities are listed in Table I, which is a summary of representative corrections and errors. Small corrections were applied to correct for the fact that the helium density is actually 0.1% larger[51] than that given by the equation of state of a perfect gas and to obtain the partial pressure of helium from the total pressure of the target gas. This partial pressure correction was made necessary by the observation in the α-particle spectra of a small number of detected particles having energies corresponding to having been scattered from nitrogen and oxygen, which presumeably represent air contamination of the target gas. The correction was made from the number of contaminant-scattered α particles by taking the cross section to be that for $\alpha + {}^{14}N$ (see Sec. II B). Normally the contaminant partial pressure amounted to several tenths of a Torr out of a total pressure of about 400 Torr, and whenever the amount of contaminant was observed to be much larger than this, the gas cell was emptied, pumped, and refilled. The contaminant partial pressure was determined to ±40%.

Local beam heating of the target gas is expected to be very small in the present experiment and only to cause local temperature changes which are well within the quoted error in target temperature. This expectation has been verified[36] by measuring

TABLE I. Representative corrections to and errors in $\alpha + \alpha$ differential cross sections. Errors are standard deviations.

Item	Correction (%)	Error (%)	Remarks
G_{00}	$\cdots$	±0.23	Scale error
Gas pressure	$\cdots$	±0.1	Scale error
Gas temperature	$\cdots$	±0.1	Scale error
Gas purity	+0.1	±0.04	Scale error
^{4}He equation of state	−0.1	$\cdots$	
Beam-charge collection	$\cdots$	±0.1	Scale error
Counting statistics	$\cdots$	±0.4	Varies
Background subtraction	$\cdots$	±0.1	Varies
Electronic dead time	+1.2	±0.05	Varies
Slit scattering	−0.15	±0.03	
Detector efficiency	+0.15	±0.06	Varies
Angular asymmetry	$\cdots$	±0.02	Larger at deep minima
Absolute angle	$\cdots$	±0.80	Varies widely
$|G/G_{00}|$	0.1	$\cdots$	Larger at deep minima
Beam shape	$\cdots$	0.0	Nonzero at deep minima

the same cross section at several beam currents encompassing a fourfold range.

The uncorrected number of detected α particles was determined from the data-detector α-particle spectrum by the subtraction of a background, mainly due to slit scattering, from the prominent spectral peak produced by $\alpha + \alpha$ scattering. This background was obtained by an extrapolation of the spectrum on the low-energy side of the $\alpha + \alpha$ peak toward higher energies in such a way that the extrapolated background became zero at the high-energy side of the $\alpha + \alpha$ peak. This was accomplished with a light pen and oscilloscope display. Typically, the subtracted background amounted to 0.5% of the number of counts in the $\alpha + \alpha$ peak and could be determined to about $\pm 20\%$. Subsequently, calculations were carried out on effects of slit-edge scattering[52] in order to help determine whether or not the extrapolation procedure was a reasonable one. The question is difficult to answer; however, it was estimated that an additional subtraction of $0.15 \pm 0.03\%$ of the number of counts in the $\alpha + \alpha$ peak should be made. This correction is the item slit scattering in Table I.

Correction for the ADC dead time has been mentioned in Sec. II A, and in addition, small corrections for the dead time of the other electronic components have been calculated from the observed counting rate. The dead-time corrections typically fall in the range 1 to 2% and are known to about $\pm 5\%$.

A small fraction of the α particles incident on the silicon detector will undergo nuclear reactions with the detector material, and most of these reactions will result in an energy deposit in the detector different from that produced by those many particles which deposit their energy through ionization processes. The magnitude of this effect will depend upon the energy of the incident α particles. A correction factor was calculated by using the $\alpha + Si$ dE/dx vs energy relation[53] and an $\alpha + Si$ total reaction cross section σ_R vs energy relation derived from optical-model calculations.[54] The correction[55] varies from 0.01 to 0.3% for the present experiment, and we assign an uncertainty of $\pm 40\%$ to this correction.

Tests for the influence of multiple Coulomb scattering in the target exit foil on the number of detected α particles have been made earlier.[36] In these tests a lower α-particle energy and thicker Kapton foils were used than were used here. The results of the tests indicate that such scattering effects are small in the present experiment and that it is reasonable to assume that the loss of particles by out-scattering is com-

pletely compensated by the gain of particles by in-scattering. Therefore, no corrections for multiple Coulomb scattering were applied to the present data.

Because of deviations of the beam direction from the optically defined line, the scattering angle is not known as accurately as the optical alignment would indicate. In order to correct for this to a large extent, the data taken left and right of the beam (see Sec. II B) were always averaged. Thus, if $\Delta \theta_b$ is the small angle which the beam makes with the optical line, then the averaging process eliminates errors due to odd powers of $\Delta \theta_b$; that is

$$\tfrac{1}{2}[\sigma(\text{left}) + \sigma(\text{right})] = \sigma_L(\theta_L) + A_2(\theta_L)\Delta\theta_b^2$$
$$+ A_4(\theta_L)\Delta\theta_b^4 + \cdots, \qquad (2)$$

where $\sigma_L(\theta_L)$ is the lab differential cross section at angle θ_L, and θ_L is the turntable angle. The term $A_2(\theta_L)\Delta\theta_b^2$ in Eq. (2) was evaluated using $\Delta\theta_b = 0.1°$ and was included in the cross-section relative error. It contributes only a very small amount to the final error and is labeled angular asymmetry in Table I. In addition, an error is present because θ_L has an uncertainty $\Delta\theta_L$ of $\pm 0.03°$ (see Sec. II A). It is convenient to express this uncertainty as an error in the cross section rather than in the angle. Therefore, we assign a further relative error to $\sigma_L(\theta_L)$ of $\sigma'(\theta_L)\Delta\theta_L$, where the prime denotes differentiation with respect to lab angle θ_L. This term often contributes a significant amount to the final relative error and is termed absolute angle in Table I.

Initially, cross sections were evaluated from Eq. (1) with the geometry factor G taken to be the zeroth-order value G_{00}, where

$$G_{00} = \frac{4abl}{hR_0} . \qquad (3)$$

The symbols in Eq. (3) have been defined in Sec. II A. To correct the data for finite angular resolution and beam geometry, higher-order terms in G must be used. When G is evaluated through terms of second order in small quantities, it can be written in the form

$$G = G_{00}\left(1 + \Delta_0 + \frac{\sigma_L'}{\sigma_L}\Delta_1 + \frac{\sigma_L''}{\sigma_L}\Delta_2\right), \qquad (4)$$

where the primes indicate differentiation with respect to lab angle θ_L. The quantities Δ_0, Δ_1, and Δ_2 are angle dependent and have been calculated[56] by Kan[49] for the detection geometry of the present experiment with a divergent beam, the model for which we discuss in the Appendix. Equations (1), (3), and (4) can be used to make

TABLE II. Measured $\alpha + \alpha$ c.m., elastic differential cross sections $\sigma_{c.m.}$ in mb/sr and their relative standard deviations Δ in percent. There is an additional 0.30% standard deviation in the absolute cross-section scale. The c.m. and lab energies are given in MeV. The cross sections have been corrected for finite angular resolution. For ease in tabulation, the c.m. scattering angle $\theta_{c.m.}$ in degrees has been decomposed into its integer part $i_{c.m.}$ and its decimal part $d/100$; thus $\theta_{c.m.} = i_{c.m.} + d/100$.

Energy	18.00 (lab) 9.00 (c.m.)			21.12 (lab) 10.55 (c.m.)			24.11 (lab) 12.04 (c.m.)			25.50 (lab) 12.74 (c.m.)			26.99 (lab) 13.48 (c.m.)			28.50 (lab) 14.24 (c.m.)			29.50 (lab) 14.74 (c.m.)		
$i_{c.m.}$	d	$\sigma_{c.m.}$	Δ (%)	d	$\sigma_{c.m.}$	Δ (%)	d	$\sigma_{c.m.}$	Δ (%)	d	$\sigma_{c.m.}$	Δ (%)	d	$\sigma_{c.m.}$	Δ (%)	d	$\sigma_{c.m.}$	Δ (%)	d	$\sigma_{c.m.}$	Δ (%)
22	3	961.9	0.37	3	1227.8	0.57	4	2017	0.75	...	...	...	4	1899	0.81	...	...	...	4	1523	0.78
24	3	856.0	0.49	3	1030.4	0.67	4	1540	0.95	4	1578	0.94	4	1471	0.93	4	1280	0.90	5	1164	0.89
26	3	747.8	0.47	4	831.9	0.76	4	1125	1.06	4	1154	1.09	5	1070	1.07	5	936.9	1.04	5	885.9	1.00
28	3	652.9	0.51	4	667.7	0.84	4	781.0	1.25	5	759	1.35	5	719.9	1.29	5	667.2	1.18	5	616.1	1.17
30	4	557.6	0.55	4	523.6	0.88	5	504.4	1.50	5	485.6	1.60	5	466.6	1.54	6	440.6	1.39	6	422.6	1.34
32	4	478.1	0.63	4	398.0	0.96	5	296.2	1.83	5	272.8	2.02	6	272.4	1.85	6	269.5	1.66	6	270.0	1.51
34	4	399.9	0.62	5	302.1	0.86	5	152.5	2.29	6	127.0	2.73	6	131.4	2.51	6	152.4	1.91	6	160.2	1.71
35	...	...	...	5	269.4	0.91	...	...	...	...	...	...	...	...	...	...	...	...	...	...	...
36	4	328.0	0.65	5	237.5	0.92	5	67.2	2.70	6	38.7	4.52	6	49.0	3.53	6	77.4	2.13	7	91.5	1.75
37	...	...	...	...	...	...	6	44.4	2.47	6	14.8	6.88	...	...	...	...	...	...	...	...	...
38	4	270.9	0.70	5	188.8	0.71	6	31.86	1.58	6	3.48	11.3	6	15.01	3.55	7	40.30	1.63	7	55.53	1.32
39	...	...	...	...	...	...	6	28.33	0.78	6	1.42	11.8	...	...	...	...	...	...	...	...	...
40	4	219.2	0.70	5	164.8	0.65	6	34.52	1.70	6	7.85	7.29	7	13.25	2.97	7	33.55	0.86	7	44.68	0.54
42	5	181.4	0.75	5	154.05	0.47	6	65.8	1.86	7	39.3	3.13	7	37.42	2.60	7	47.01	1.38	8	52.96	0.93
43	...	...	...	...	...	...	6	87.7	1.67	...	...	...	...	...	...	...	...	...	...	...	...
44	5	145.6	0.78	...	...	...	...	...	...	7	87.7	1.81	7	74.86	1.73	8	72.40	1.27	8	71.74	1.03
45	...	...	...	6	155.02	0.49	7	141.3	1.21	...	...	...	...	...	...	...	...	...	...	...	...
46	5	120.24	0.74	...	...	...	7	166.4	0.99	7	144.5	1.14	7	119.1	1.14	8	103.89	0.94	8	95.44	0.87
47	...	...	...	...	...	...	7	192.6	0.92	...	...	...	...	...	...	...	...	...	...	...	...
48	5	97.60	0.73	6	168.51	0.45	...	...	...	7	195.0	0.76	8	162.5	0.81	8	133.58	0.70	8	118.46	0.69
50	5	79.81	0.72	6	176.70	0.27	7	260.2	0.59	8	238.2	0.52	8	194.8	0.58	8	156.68	0.54	9	135.58	0.50
52	5	69.17	0.60	6	181.92	0.44	...	...	...	8	265.7	0.38	8	218.24	0.44	9	171.62	0.42	9	145.62	0.38
53	...	...	...	...	...	...	7	301.6	0.40	...	...	...	...	...	...	...	...	...	...	...	...
54	6	60.35	0.57	7	181.34	0.44	...	...	...	8	281.0	0.42	8	224.62	0.27	9	175.30	0.46	9	147.60	0.49
55	...	...	...	7	182.45	0.54	8	305.02	0.28	...	...	...	...	...	...	...	...	...	...	...	...
56	6	56.78	0.51	7	176.21	0.48	8	300.7	0.36	8	277.7	0.37	9	223.10	0.36	9	169.04	0.52	9	139.86	0.51
58	6	54.64	0.48	7	167.30	0.40	8	285.3	0.38	8	258.1	0.42	9	203.38	0.46	9	154.09	0.61	10	127.10	0.65
60	6	55.79	0.53	7	154.43	0.44	8	254.7	0.59	9	230.9	0.66	9	181.1	0.65	10	132.41	0.74	10	107.83	0.74
62	6	60.18	0.53	7	141.27	0.61	8	217.5	0.67	9	193.0	0.79	9	147.5	0.83	10	107.42	0.89	10	86.66	0.92
64	6	65.85	0.56	7	120.32	0.64	8	173.8	0.90	9	152.8	0.89	9	115.1	0.97	10	83.09	1.01	10	66.11	1.04
65	...	...	...	7	114.01	0.71	...	...	...	...	...	...	...	...	...	...	...	...	...	...	...
66	6	74.78	0.57	...	...	...	8	131.43	1.06	9	114.2	1.08	10	85.19	1.14	10	61.26	1.04	10	48.49	1.05
68	6	84.77	0.60	8	87.89	0.67	9	91.5	1.32	9	78.0	1.33	10	60.69	1.15	10	44.91	0.98	11	37.43	0.82
70	7	97.20	0.62	...	...	...	9	57.38	1.67	9	50.41	1.51	10	43.14	1.02	11	37.59	0.59	11	33.77	0.54
72	7	110.83	0.59	8	64.23	0.65	9	31.26	2.18	9	31.76	1.43	10	36.19	0.57	11	38.84	0.69	11	38.34	0.87
73	...	...	...	...	...	...	9	20.63	2.61	...	...	...	...	...	...	...	...	...	...	...	...
74	7	126.28	0.55	...	...	...	9	13.28	3.00	9	22.91	0.82	10	37.65	0.71	11	48.38	0.97	11	50.70	1.07

TABLE II (Continued)

$\theta_{c.m.}$	18.00 (lab) 9.00 (c.m.)			21.12 (lab) 10.55 (c.m.)			24.11 (lab) 12.04 (c.m.)			25.50 (lab) 12.74 (c.m.)			26.99 (lab) 13.48 (c.m.)			28.50 (lab) 14.24 (c.m.)			29.50 (lab) 14.74 (c.m.)		
	d	$\sigma_{c.m.}$	$\Delta\,(\%)$	d	$\sigma_{c.m.}$	$\Delta\,(\%)$	d	$\sigma_{c.m.}$	$\Delta\,(\%)$	d	$\sigma_{c.m.}$	$\Delta\,(\%)$	d	$\sigma_{c.m.}$	$\Delta\,(\%)$	d	$\sigma_{c.m.}$	$\Delta\,(\%)$	d	$\sigma_{c.m.}$	$\Delta\,(\%)$
75	···	···	···	8	54.57	0.61	9	8.26	3.28	9	22.03	0.57	···	···	···	···	···	···	···	···	···
76	7	138.16	0.52	···	···	···	9	4.63	3.28	10	22.88	0.76	10	48.13	1.01	11	66.38	1.04	11	70.82	1.05
77	···	···	···	···	···	···	9	3.042	1.89	···	···	···	···	···	···	···	···	···	···	···	···
78	7	152.67	0.49	8	51.79	0.47	···	···	···	10	31.45	1.14	10	66.56	0.95	11	89.86	0.93	11	95.55	0.93
80	7	165.18	0.47	8	53.33	0.41	9	7.79	2.63	10	45.51	1.07	10	88.04	0.85	11	118.09	0.80	11	124.2	0.82
82	7	177.75	0.38	8	56.73	0.48	9	16.87	1.66	10	61.76	0.86	10	111.63	0.74	11	144.87	0.68	11	153.4	0.69
84	7	189.06	0.43	8	59.67	0.48	9	25.81	1.12	10	78.54	0.73	10	134.21	0.56	11	170.0	0.63	11	177.5	0.58
85	···	···	···	8	61.93	0.58	···	···	···	···	···	···	···	···	···	···	···	···	···	···	···
86	7	193.00	0.36	8	63.12	0.47	9	35.22	0.79	10	92.16	0.59	10	152.13	0.55	11	188.6	0.54	11	197.0	0.52
88	7	198.71	0.42	8	64.01	0.51	9	39.67	0.54	10	100.24	0.48	···	···	···	11	202.02	0.49	11	209.74	0.46
90	7	199.16	0.42	8	64.51	0.75	9	42.67	0.50	10	104.19	0.44	10	168.05	0.45	11	204.4	0.50	11	211.2	0.50

self-consistent corrections for finite angular resolution. We chose to do this in combination with the phase-shift analysis discussed in Sec. IV, because analytical expressions for σ_L' and σ_L'' to be used in Eq. (4) can be obtained directly from the formula for $\sigma_L(\theta_L)$ in terms of the phase shifts. Accordingly, the following procedure was carried out. The initial cross section values $\sigma_L(\theta_L)$ obtained by using Eq. (3) were subjected to a least-squares phase-shift fit. The resultant phase shifts were used to obtain σ_L' and σ_L'', which were then used in Eq. (4) to obtain G at each angle θ_L. With these G values, new values for $\sigma_L(\theta_L)$ were obtained and the procedure was iterated until convergence occurred. We found that, with our data, one iteration was sufficient to obtain convergence. The difference between the final values of G and the value of G_{00} is generally less than a few tenths of a percent (see $|G/G_{00}|$ in Table I); however, near deep minima the difference becomes several percent. Uncertainties in G introduced by reasonable variations in beam shape parameters (see the Appendix) are generally negligible, but rise to a maximum of 1% at deep minima. These uncertainties are included in the cross-section relative errors.

The beam energy at the center of the gas target, the reaction energy, is known to ±18 keV. This uncertainty arises both from the uncertainty in the beam energy calibration (see Sec. II A) and from the uncertainty in the calculation of the beam energy loss in the cell foil and ^{4}He gas. The energy spread in the beam at the cell center is ±33 keV full width at half maximum (FWHM) and is almost entirely due to straggling in the cell foil.

The final lab differential cross sections, lab angles, and reaction energies were converted to the c.m. system by use of fully relativistic formulas. The total error in cross-section absolute scale is 0.30%, which is the sum in quadrature of the contributions labeled scale error in Table I, and the total relative error is the sum in quadrature of the contributions from the remaining items in Table I. The c.m. differential cross sections are listed in Table II and are plotted in Fig. 1.

IV. PHASE-SHIFT ANALYSIS

The extraction of phase shifts from the present data is greatly simplified by the fact that the $\alpha + \alpha$ system consists of identical, spin-zero particles and by the fact that there are no open reaction channels in the energy region investigated here. Thus, the phases exist only for even values of the orbital angular momentum l and are purely real. Furthermore, at the present

energies only a small number of phase shifts will
be nonzero.

The expression $\sigma(\theta, \delta)$ for the $\alpha + \alpha$ c.m. dif-
ferential cross section in terms of the phase
shifts δ_l is well known[17,18] and will not be written
down here. At each bombarding energy the phase
shifts are determined by minimizing[57] the function
χ^2 defined by

$$\chi^2 = \sum_{i=1}^{N_d} \left[\frac{\gamma\sigma(\theta_i, \delta) - \sigma(\theta_i)}{\Delta\sigma_i} \right]^2 + \left(\frac{\gamma - 1}{\Delta\gamma} \right)^2 , \quad (5)$$

where N_d is the number of data points comprising

the angular distribution, the θ_i are the c.m. angles
at which the data were obtained, $\sigma(\theta_i)$ is the mea-
sured c.m. differential cross section, $\Delta\sigma_i$ is the
relative standard deviation of $\sigma(\theta_i)$, $\Delta\gamma = 0.003$
is the fractional experimental error in the cross-
section absolute scale, and γ is a normalization
factor, which is varied along with the phase shifts
to minimize χ^2 and which is introduced to aid in
exposing possible hidden systematic errors in
the data. If such errors are not very significant,
we would expect that the majority of the γ values
determined from the χ^2 minimization would fall
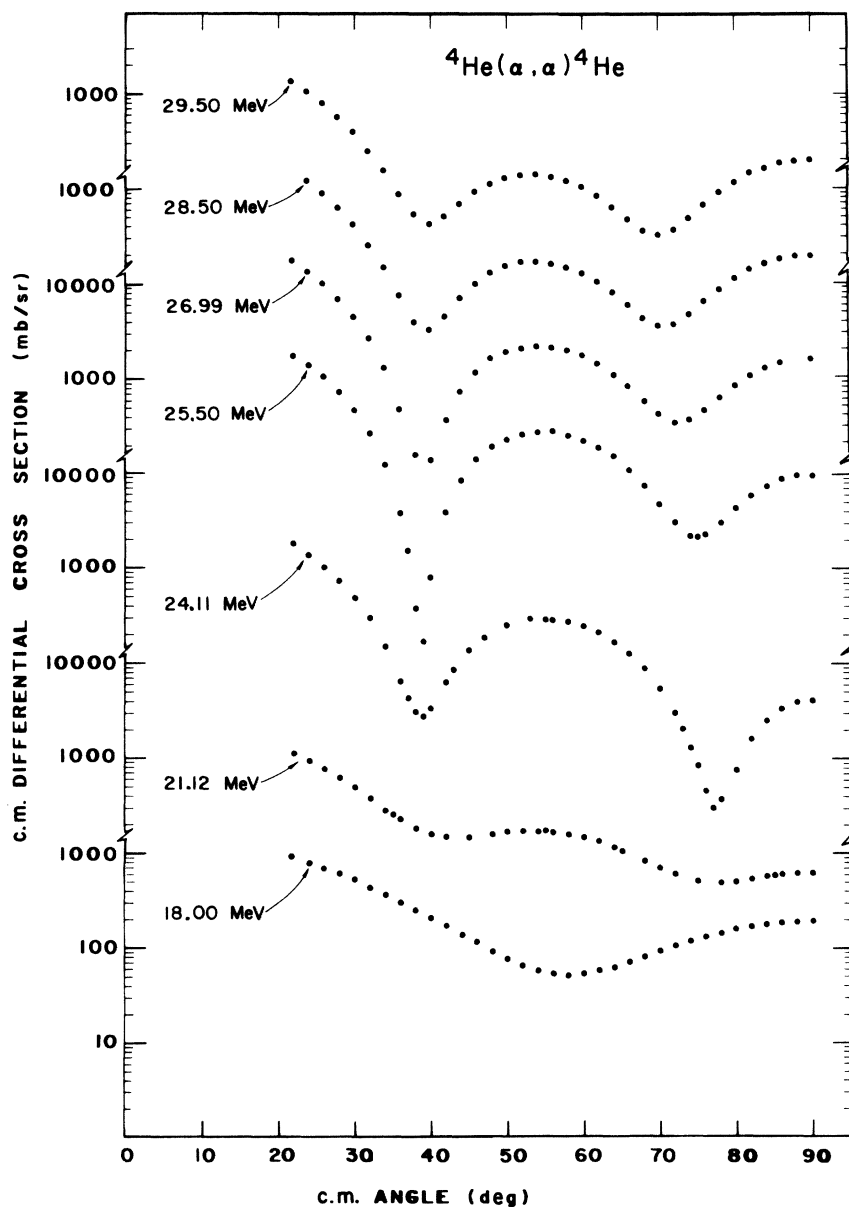
FIG. 1. c.m. differential cross sections for $\alpha+\alpha$ elastic scattering measured in the present work. Lab energies are
indicated, and almost every plotted point is larger in size than its associated error.

in the range 0.997 to 1.003. Indeed, Fig. 2 does show that the obtained γ values are consistent with the assigned scale error.

The method used to minimize χ^2 is described in Ref. 58 under the subheading square matrix search. Continuity of the phase shifts as a function of energy was used to determine starting values for the phases, and convergence from these starting values to values yielding a χ^2 minimum was rapid. The same χ^2-minimizing solutions were obtained when several other sets of starting values were used; however, no attempt was made to perform an exhaustive search for other local minima in χ^2 space. In Table III are listed the obtained phase shifts δ_l, normalization factors γ, and values of χ^2 per degree of freedom ν (ν is 5 or 6 less than N_d). The quoted errors are the square roots of the diagonal elements of the standard error matrix.[58] These errors do not indicate how strong correlations between different fitting parameters might be. Such correlations are measured by the off-diagonal elements of the error matrix, and many of these elements were found[30] to have values not greatly different from the values of the diagonal elements. This latter fact implies that correlations are often significant.

The largest angular-momentum value l_m used in the fitting procedure for the phases of Table III was $l_m = 6$ for the three lowest energies and $l_m = 8$ for the four highest energies. In addition, fits were carried out using $l_m = 8$ at the three lowest energies and $l_m = 6$ at the four highest energies. Except for the data at 25.50 MeV (lab), the phase shifts obtained using $l_m = 6$ differ only slightly from those obtained using $l_m = 8$. At 25.50 MeV (lab), however, this difference is significant; for example, the fit for $l_m = 6$ gives the value $\delta_4 = 85.57° \pm 0.40°$, which is not only smaller by $3.07° \pm 1.81°$ than the value in Table III, but also has a considerably smaller associated error. Such behavior can
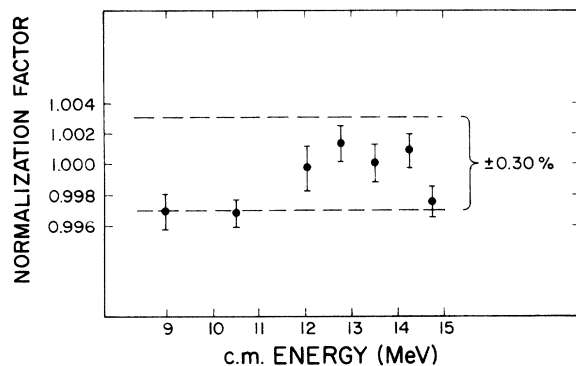
FIG. 2. Normalization factor γ from Table III. The dashed lines indicate the standard deviation associated with the cross-section scale.

be verified by an inspection of the error matrices for $l_m = 8$, which show[30] that the correlations between δ_8 and the other δ_l are at least 10 times stronger at 25.50 MeV (lab) than at any other energy. Thus, at this energy even a small value for δ_8 and its associated error can produce significant effects on the other phases. Even though we expect on physical grounds that δ_8 should be very near zero in the present energy region, we have nevertheless chosen to present, at 25.50 MeV (lab), the phase-shift set obtained when δ_8 was included in the fitting procedure. We feel that had we excluded δ_8, thereby ignoring the correlations inherent in our data, the resultant phase-shift errors would have been unrealistically small.

A simple test was carried out on the 25.50-MeV (lab) data to attempt to discover whether or not the correlations with δ_8 arise from data in a narrow angular region rather than being associated with the entire angular distribution. The errors of a data group at five successive angles were multiplied by a factor of 4, and then a phase-shift analysis was performed for each angular position of the data group. The angular position was varied to cover the entire angular distribution; however, no significant changes in the correlations were produced by this procedure. In particular, the effective removal of the data points around the deep minimum near 40° (c.m.) had no effect. We presume that removal of the δ_8 correlations at this energy would require more accurate measurements than we have made here.

V. THEORETICAL INTERPRETATIONS

A. R-matrix analysis of δ_4

The R-matrix formalism[59] is often used to extract nuclear parameters from experimental data on resonance reactions; for example, in Refs. 7 and 8 this formalism is applied to a study of 0^+ and 2^+ levels in ^{8}Be. In Ref. 15 a single-level analysis of δ_4 for the $\alpha + \alpha$ system was made using the limited data then available ($E_{lab} < 23$ MeV, $\delta_4 < 60°$). With the inclusion of the δ_4 values from the present experiment with others available,[15-17] a more accurate analysis is possible.

In the energy range we use to analyze δ_4, only the elastic channel is open; consequently the R matrix becomes an R function. Because we consider only $l = 4$, we sometimes suppress reference to l in the following formulas. The nuclear phase shift δ_4 is expressed as

$$\delta_4 = -\phi_4 + \tan^{-1}\left[\frac{RP_4}{1 - R(S_4 - B)}\right] , \qquad (6)$$

where R is a sum over levels λ and involves the

TABLE III. $\alpha + \alpha$ phase shifts δ_l, normalization factor γ, and χ^2 per degree of freedom ν obtained from analysis of the differential cross sections of this work. The indicated errors are the diagonal elements of the standard error matrix.

E_{lab} (MeV)	$E_{c.m.}$ (MeV)	χ^2/ν	γ	δ_0 (deg)	δ_2 (deg)	δ_4 (deg)	δ_6 (deg)	δ_8 (deg)
18.00	9.00	1.64	0.9970 ± 0.0010	7.14 ± 0.15	101.38 ± 0.21	15.86 ± 0.12	0.60 ± 0.11	$\cdots$
21.12	10.55	2.28	0.9967 ± 0.0009	-4.96 ± 0.14	96.33 ± 0.07	36.27 ± 0.07	0.54 ± 0.05	$\cdots$
24.11	12.04	1.21	0.9997 ± 0.0014	-15.33 ± 0.16	91.86 ± 0.13	72.61 ± 0.16	0.87 ± 0.06	$\cdots$
25.50	12.74	0.68	1.0013 ± 0.0012	-19.64 ± 1.01	89.37 ± 1.54	88.64 ± 1.77	1.61 ± 0.39	0.36 ± 0.19
26.99	13.48	1.09	1.0002 ± 0.0013	-22.81 ± 0.96	88.98 ± 0.63	105.29 ± 0.88	1.56 ± 0.17	0.05 ± 0.11
28.50	14.24	0.29	1.0006 ± 0.0012	-27.03 ± 0.30	86.79 ± 0.15	115.26 ± 0.20	1.70 ± 0.10	-0.03 ± 0.09
29.50	14.74	0.68	0.9976 ± 0.0010	-29.12 ± 0.17	86.90 ± 0.13	121.19 ± 0.17	2.20 ± 0.11	0.11 ± 0.08

$l = 4$ level energies E_λ and $l = 4$ reduced widths γ_λ^2;

$$R = \sum_\lambda \frac{\gamma_\lambda^2}{E_\lambda - E} \quad . \qquad (7)$$

In Eq. (6) P_l, $-\phi_l$, and S_l ($l = 4$) are the penetration factor, hard-sphere phase shift, and shift factor, respectively. Expressions for these are given in Ref. 59, and they depend on wave number k, Coulomb parameter η, and a channel radius parameter a. The constant B in Eq. (6) is a boundary condition parameter.

The resonance energy $E_{r\lambda}$ for a level λ is defined[59] as that energy at which the level's resonance contribution to the phase shift would be an odd integral multiple of $\frac{1}{2}\pi$ were that level the only one present; that is

$$E_{r\lambda} = E_\lambda + \Delta_\lambda \ , \qquad (8)$$

where the $l = 4$, energy-dependent level shift Δ_λ is given by

$$\Delta_\lambda = -\gamma_\lambda^2 (S_4 - B). \qquad (9)$$

This definition of resonance energy has the property that if the constant B is chosen as $B = S_l(E_{r\lambda_1})$, thereby making the level shift for the particular level λ_1 zero at its resonance energy $E_{r\lambda_1}$, then the *total* resonant phase shift $\delta_l + \phi_l$ is an integral multiple of $\frac{1}{2}\pi$ at $E = E_{r\lambda_1}$, whether or not other levels contribute to R.

As a first step in analyzing the $l = 4$ phase shifts, we have performed a single-level ($\lambda = 1$ only), least-χ^2 fit to the $l = 4$ phases of Ref. 15. We have taken the channel radius to be $a = 4.4$ fm as in Ref. 15 and have set[60] $B = 0$. The fit yields $E_{r1} = 11.7$ MeV, $\gamma_1^2 = 1.46$ MeV, and a level width $\Gamma_1 = 2\gamma_1^2 P_4 = 6.3$ MeV. These values differ somewhat from those quoted in Ref. 15; however, both these parameters and those of Ref. 15 fit only the low-energy part of the δ_4 resonance structure and fail completely to fit δ_4 over an energy range which includes the present data; this fact is illustrated by the dashed curve in Fig. 3. Furthermore, no

acceptable, single-level fit to δ_4 was found possible over the energy range of Fig. 3. Such a failure is a common problem[19] which arises in fitting broad levels; that is, the hard-sphere phase is not an adequate representation of the nonresonant part of the phase shift over a sufficient energy range.[61] One method of solving this problem is to parametrize ϕ_l as an energy-dependent nonresonant phase and to determine the parameters during the χ^2 fitting procedure. Here we adopt a different method, that of representing
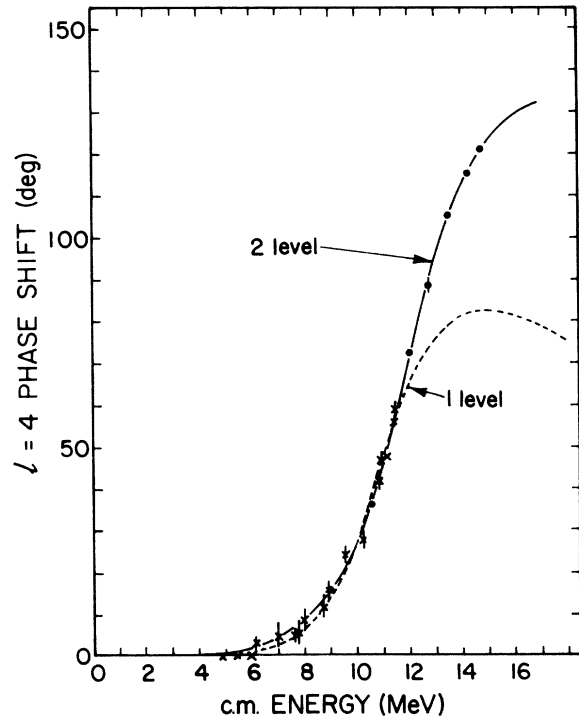
FIG. 3. R-matrix fits to δ_4. The points represent the $\alpha + \alpha$ phase shifts determined in the present work, and the crosses are from Refs. 15–17. The dashed curve is a one-level fit to the phase shifts of Ref. 15, and the solid curve is a two-level fit to all the phases shown.

the nonresonant phase by an artificial second "level." Thus we have performed a two-level fit in which $\lambda = 1$ represents the physical resonance near 12 MeV and $\lambda = 2$ represents a background phase produced by the cumulative effects of other $l = 4$ levels.

In the two-level fit, the channel radius a was chosen by studying[30] how the best-fit value of χ^2 varies as a function of a and by choosing a to be in the rather broad minimum which exists in the χ^2 vs a relation. The parameter B was chosen such that the level shift at the $\lambda = 1$ resonance energy is zero; a procedure which discussions in Refs. 7 and 62 indicate is a reasonable one and which was mentioned immediately after Eq. (9). The final fit, which yields the quite satisfactory value for χ^2 per degree of freedom of 1.6 and which is illustrated in Fig. 3, was generated by the following parameters:

$$a = 4.4 \text{ fm}, \quad B = -1.0434,$$

$$E_{r1} = E_1 = 11.68 \text{ MeV}, \quad \gamma_1^2 = 0.97 \text{ MeV},$$

$$E_2 = 58.9 \text{ MeV}, \quad \gamma_2^2 = 10.0 \text{ MeV}.$$

The level width computed from $\Gamma_1 = 2\gamma_1^2 P_4$, where P_4 is evaluated at 11.68 MeV, has the value 4.0 MeV. An alternate level-width definition,[7] which allows for the variation of the level shift with energy, is that Γ_λ is the difference between the energy at which the resonant phase for $\lambda = 1$ alone equals 135° and the energy at which it equals 45°. This definition yields $\Gamma_1 = 3.8$ MeV. The reduced width of 0.97 MeV from the two-level analysis is 60% of the Wigner limit and is significantly smaller than the reduced width from the single-level analysis, which is 92% of the Wigner limit.

Finally, if we take into consideration variations in the level parameters with channel radius, we can quote an associated uncertainty:

$$l = 4 \text{ resonance energy} = 11.0 \pm 0.4 \text{ MeV},$$

$$l = 4 \text{ level width} = 4.0 \pm 0.4 \text{ MeV}.$$

B. Comparison with resonating-group calculations

The resonating-group method[23] has had considerable success in calculations of properties of light nuclear systems. In particular, this method often has been applied to the $\alpha + \alpha$ system,[9-12] because it is expected that this system should be very useful for testing such calculations, especially at energies below the first reaction threshold. In Fig. 4 we compare the present phase shifts and others[15-18] in the energy range 1.5 to 15 MeV (c.m.) with recent resonating-group calculations.[11,12] The solid curves are from the calculation of Niem, Heiss, and Hackenbroich.[12] This

calculation includes a soft repulsive core in the employed nucleon-nucleon potential and includes effects of the $\alpha + \alpha^*$ channel, where α^* denotes the first excited $T = 0$, $J^\pi = 0^+$ state of the α particle. It is seen from Fig. 4 that this calculation does quite well in reproducing the experimentally determined phase shifts. Also illustrated in Fig. 4 are $l = 4$ phase shifts (dashed curve) calculated[11] in a single-channel approximation with no repulsive core in the nucleon-nucleon potential. The $l = 0$ and $l = 2$ phase shifts (not shown) from this calculation are very similar to those of Ref. 12; however, the $l = 4$ phase shift disagrees both with experiment and with the calculation of Ref. 12. The fact that disagreement occurs for δ_4, but not for δ_0 and δ_2, may seem puzzling at first, because both the $\alpha + \alpha^*$ channel[63] and the nucleon-nucleon repulsive core produce effects which become progressively weaker as the angular momentum increases. It must be realized, however, that in the calculation of Ref. 11 an adjustment[64] was made in the nucleon-
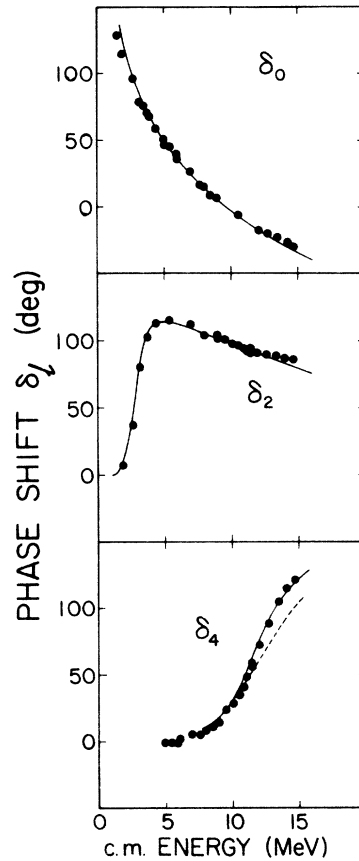
FIG. 4. Comparison of the $\alpha + \alpha$ phase shifts determined in the present work and those of Refs. 15–18 with resonating group calculations. The solid curves represent the calculations of Ref. 12, and the dashed curve represents the δ_4 calculation of Ref. 11.

nucleon exchange constant u [see Eq. (2) of Ref. 11]. This adjustment is not able to compensate completely for the differences between the calculations of Refs. 11 and 12. The particular value of u used in Ref. 11 causes the disagreement to appear in δ_4; however, a slightly larger value of u would cause the δ_4 calculations to approach agreement and would cause instead a disagreement in both δ_0 and δ_2. Such a disagreement in δ_0 and δ_2 would then be in the right direction to be caused by the use of a nucleon-nucleon repulsive core in one calculation but not in the other.

C. Potential-model analysis

Phenomenological nuclear potentials $V_{\alpha\alpha}$ describing the $\alpha+\alpha$ interaction[3,5,6,19] have applications in several areas[3]; however, here we are primarily interested in an aspect of $V_{\alpha\alpha}$ which was discussed by Ali and Bodmer,[3] namely, the possibility that an accurate determination of its long-range part might yield some information on the spin-isospin independent part (direct part) of the nucleon-nucleon potential. This possiblity occurs because, first, the fact that the α particle has $T = 0$ and $J^\pi = 0^+$ implies that the direct part V_D of $V_{\alpha\alpha}$ arises almost entirely from the direct part of the nucleon-nucleon potential, and second, theoretical studies have shown[1,2,9,10] that V_D is of longer range than the exchange part[24] of $V_{\alpha\alpha}$. More specifically, resonating-group calculations[10] indicate that exchange effects produce a short-range repulsive component in $V_{\alpha\alpha}$ for $l=0$, produce a weaker short-range repulsive component in $V_{\alpha\alpha}$ for $l=2$, and have very little influence for $l \geqslant 4$. Therefore, δ_4 is determined almost entirely by V_D. We should mention that such l-dependent characteristics of the short-range repulsive components of $V_{\alpha\alpha}$ have been found in previous studies[3,5,19] of phenomenological $\alpha+\alpha$ potentials (however, see Ref. 6).

Here we follow much of the procedure of Ali and Bodmer,[3] with two important differences, however. One difference is the practical one that a more definitive analysis of the long-range part of $V_{\alpha\alpha}$ is now possible because of the accurate results obtained for δ_4 in the present experiment; the analysis of Ref. 3 was restricted to $\delta_4 < 60°$. The other difference is that, instead of using a Gaussian form[3] for the direct part V_D of $V_{\alpha\alpha}$, we employ a folded form incorporating a direct nucleon nucleon potential of Yukawa form, which is a form more amenable to meson-theoretical interpretations.[2]

We write the potential V of the Schrödinger equation for $\alpha+\alpha$ scattering as follows:

$$V = V_{\alpha\alpha} + V_C , \tag{10}$$

where V_C is the Coulomb potential appropriate to a Gaussian density and is given by[10]

$$V_C = \frac{4e^2}{r} \Phi[(2\alpha/3)^{1/2}r] , \tag{11}$$

with

$$\Phi(x) = \frac{2}{\sqrt{\pi}} \int_0^x e^{-t^2} dt , \tag{12}$$

and where[65] $\alpha = 0.514$ fm^{-2}. The nuclear potential $V_{\alpha\alpha}$ of Eq. (10) is expressed as

$$V_{\alpha\alpha}(r) = V_r e^{-\mu_r^2 r^2} + V_D(r) , \tag{13}$$

in which the parameters V_r and μ_r of the repulsive part of $V_{\alpha\alpha}$ are l dependent, and from the above discussion, we take $V_r = 0$ for $l \geqslant 4$. The direct $\alpha+\alpha$ potential V_D of Eq. (13) is obtained by folding[66] α-particle matter densities $\rho(r)$ together with a direct nucleon-nucleon potential V_d (r);

$$V_D(r)$$
$$= \int \rho(r_1)\rho(r_2)V_d (s)\delta(\vec{r}_2 - \vec{r}_1 - \vec{s} + \vec{r}) d\vec{r}_1 d\vec{r}_2 d\vec{s}, \tag{14}$$

where $\vec{r}_1$ and $\vec{r}_2$ are measured, respectively, from the c.m. point of each α particle, and $\vec{r}$ is the vector connecting the c.m. point of one α particle with the c.m. point of the other. The α-particle densities are computed from Gaussian α-particle wave functions ψ_α; thus

$$\psi_\alpha = \exp\left[-\frac{\alpha}{2}\sum_{i=1}^{4} r_i^2\right], \quad \sum_{i=1}^{4} \vec{r}_i = 0, \tag{15}$$

and

$$\rho(r) = \left\langle \psi_\alpha \left| \sum_{i=1}^{4} \delta(\vec{r} - \vec{r}_i) \right| \psi_\alpha \right\rangle \Big/ \langle \psi_\alpha | \psi_\alpha \rangle$$
$$= 32\left(\frac{\alpha}{3\pi}\right)^{3/2} e^{-(4/3)\alpha r^2} . \tag{16}$$

The nucleon-nucleon potential is given the Yukawa form

$$V_d(r) = -\frac{V_0}{\beta r} e^{-\beta r} . \tag{17}$$

The use of Eqs. (16) and (17) in Eq. (14) yields[1]

$$V_D(r) = -V_{D0} \frac{e^{-\beta r}}{\beta r} \tfrac{1}{2}\{1 + \Phi(\lambda_-) - e^{2\beta r}[1 - \Phi(\lambda_+)]\} , \tag{18}$$

with

$$V_{D0} = 16 V_0 \exp[3\beta^2/(8\alpha)] , \tag{19}$$

and

$$\lambda_\pm = \left(\frac{2\alpha}{3}\right)^{1/2}\left(r \pm \frac{3\beta}{4\alpha}\right) . \tag{20}$$
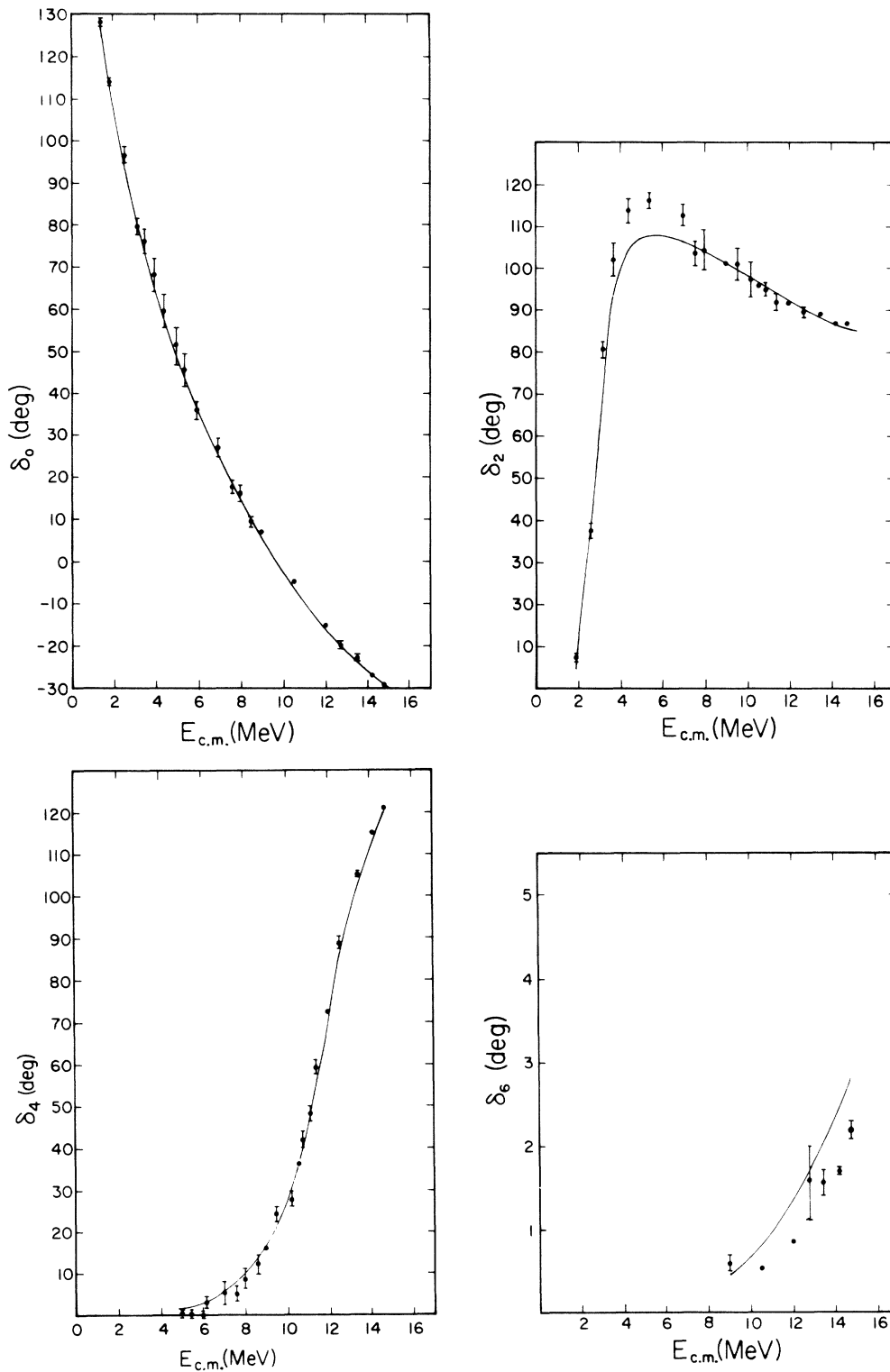
FIG. 5. Potential-model fits to the $\alpha + \alpha$ phase shifts determined in the present work and those of Refs. 15–18. The curves represent the results of using the potential parameters of Table IV.

It is of interest to present results for $V_D(r)$ for the special cases $r \to \infty$ and $r = 0$; thus

$$V_D(r) \to - V_{D0} \frac{e^{-\beta r}}{\beta r}, \quad \text{as } r \to \infty, \tag{21}$$

and

$$V_D(0) = \frac{-16 V_0}{\beta} \left(\frac{8\alpha}{3\pi}\right)^{1/2} - V_{D0} \left\{ \Phi\left[\beta\left(\frac{3}{8\alpha}\right)^{1/2}\right] - 1 \right\}. \tag{22}$$

The six parameters V_0, β, V_r ($l = 0, 2$), and μ_r ($l = 0, 2$) of the $V_{\alpha\alpha}$ of Eq. (13) were varied to carry out a least-χ^2 fit to the present $\alpha + \alpha$ phase shifts and others.[15-18] First, V_0 and β were varied to fit δ_4. Then, with V_0 and β fixed at the values so determined, V_r and μ_r were varied to fit δ_0 and then varied again to fit δ_2. The resultant parameters are listed in Table IV, the fits to the phase shifts are shown in Fig. 5, and the potential $V_{\alpha\alpha}$ is illustrated in Fig. 6.

We can compare the Yukawa potential obtained in the present analysis with nucleon-nucleon potentials which do not contain a repulsive core, but which fit the low-energy nucleon-nucleon data. There are many such potentials; we choose for comparison the potential of Reichstein and Tang[67] (RT), which has been used often in resonating-group calculations. When a pure Serber form ($u = 1$) is chosen for the RT potential, its direct part has a volume integral of 454 MeV fm³ and an rms radius of 2.06 fm. The present Yukawa potential has somewhat smaller values for these quantities: The volume integral is given by $4\pi V_0/\beta^3 = 434$ MeV fm³ and the rms radius is given by $\sqrt{6}/\beta = 1.81$ fm.

In one-boson-exchange models[68, 69] (OBEM) of the nucleon-nucleon (NN) interaction, the direct part V_d of the interaction comes from the exchange of

$T = 0$ mesons having $J^\pi = 0^+$ or 1^-. Therefore, the long-range part of the NN interaction, that part due to one-pion exchange, does not contribute to V_d. The exchange mass m associated with our Yukawa range β^{-1} is given by $mc^2 = \beta\hbar c = 266$ MeV, or

$$m = (1.97^{+0.07}_{-0.03})\mu, \tag{23}$$

where μ is the mass of the neutral pion. Thus we do find an exchange mass significantly larger than the pion mass, which fact implies a range for V_d shorter than that of the one-pion-exhange potential. However, the $T = 0$, $J^\pi = 0^+$ meson (often termed σ_0) included in OBEM in order to produce the required NN intermediate-range attraction should have a mass m_0 in the range $(3-5)\mu$ to allow a reasonable fit to empirical NN phase shifts. In addition, the dimensionless σ_0-nucleon coupling constant g_0^2 should be[68] about 10 (for $m_0 \approx 4\mu$), whereas from our potential we obtain $g^2 = V_0/[mc^2(1 - \frac{1}{4} m^2/M^2)] = 0.33$, where M is the nucleon mass. For some time there was no experimental evidence for the existence of this isoscalar-scalar meson postulated in OBEM, and in some analyses[69]

TABLE IV. Values of the Yukawa parameters (V_0, β), of the repulsive core parameters (V_r, μ_r), and of the χ^2 per degree of freedom ν obtained from fits to the phase shifts δ_l vs energy. The indicated error for a parameter corresponds to the occurence of a 50% increase in χ^2 when the other varied parameter is adjusted to maintain a relative minimum for χ^2. The results of using the tabulated parameters are illustrated in Fig. 5.

l	V_0 (MeV)	β (fm^{-1})	V_r (MeV)	μ_r (fm^{-1})	χ^2/ν	Parameters varied
0	85	1.35	287.5^{+30}_{-26}	0.635 ± 0.015	3.6	V_r, μ_r
2	85	1.35	176.5^{+18}_{-20}	0.620 ± 0.020	10	V_r, μ_r
4	85^{+9}_{-2}	$1.35^{+0.05}_{-0.02}$	0	$\cdots$	12	V_0, β
6	85	1.35	0	$\cdots$	30	None

FIG. 6. The nuclear $\alpha + \alpha$ potential $V_{\alpha\alpha}$ of Eq. (13) for the parameter values of Table IV.

a weakly interacting σ_0 ($g_0{}^2 \approx 2$, $m_0 \approx 3\mu$) was used to simulate the isoscalar part of continuum two-pion exchange effects. However, a recent analysis[70] of the $T = 0$, s-wave $\pi\pi$ phase shift yielded a solution containing a broad resonance (termed ϵ instead of σ_0) in the associated amplitude, although the authors of Ref. 70 are careful to comment that their $\pi\pi$ analysis can also yield a solution which does not contain an ϵ resonance. It is definitely concluded,[70] however, that if the ϵ meson exists then it must be broad—no narrow ϵ resonance is possible in the energy range investigated. The results of Ref. 70 have been incorporated[71] into a OBEM of all the experimentally studied baryon-baryon systems; the parameters used were[72] $m_\epsilon c^2 = 670$ MeV, $\Gamma_\epsilon = 500$ MeV, $g_\epsilon{}^2 = 16.23$. The width Γ_ϵ of the ϵ meson was taken into account in that analysis, whereas in earlier OBEM it was usual procedure to neglect all widths.[73] It is possible that the small values for m and g^2 associated with the potential we extract from $\alpha + \alpha$ scattering data is a manifestation of the low-mass region of the ϵ-meson mass distribution.[74] This question certainly deserves further study.

VI. CONCLUSION

Accurate measurements have been made of differential cross sections for $\alpha + \alpha$ elastic scattering in the energy range from 9 to 15 MeV (c.m.). A phase-shift analysis was performed on the data, and the resultant phase shifts, along with others from the literature, were used to study the $\alpha + \alpha$ system over a wide energy range below the first reaction threshold.

A two-level R-matrix analysis of δ_4 was made in which one level represents the physical resonance near 12 MeV (c.m.) and the other level represents the contribution to the nonresonant background phase from the cumulative effects of higher-energy $l = 4$ levels. This method of analysis, in combination with the inclusion in the analysis of the present accurate values for δ_4, has resulted in a rather reliable determination of the width of the first $J^\pi = 4^+$ state in ^{8}Be.

We have compared the $\alpha + \alpha$ phase shifts with those calculated with the resonating-group method. The comparison indicates that in the calculation it is necessary to take account of the short-range repulsion in the nucleon-nucleon interaction.

A potential-model fit has been made to the $\alpha + \alpha$ phase shifts with the aim of obtaining some information on the spin-isospin independent part V_d of the nucleon-nucleon potential. It is expected that V_d will make the major contribution to the long-range attractive part of the $\alpha + \alpha$ potential $V_{\alpha\alpha}$. This long-range attractive part of $V_{\alpha\alpha}$ was obtained by folding Gaussian α-particle matter

densities together with a direct nucleon-nucleon potential V_d of Yukawa form. Phenomenological short-range repulsive components were included in $V_{\alpha\alpha}$ for $l = 0$ and $l = 2$ in order to account for exchange effects.[75] The strength and range of the Yukawa V_d obtained from the fitting procedure were discussed in terms of one-boson-exchange models of the nucleon-nucleon interaction. It was concluded that an important future improvement in the analysis would be to take account of the large width of the isoscalar-scalar meson whose exchange should dominate the long-range part of V_d and, hence, the long-range part of $V_{\alpha\alpha}$.

Finally, we comment on several other improvements in the present potential analysis, which could lead to a better understanding of the relationship between V_d and $V_{\alpha\alpha}$. The question of precisely how much influence exchange processes have on the long-range part of $V_{\alpha\alpha}$ should be investigated; the resonating-group method appears to be particularly suited for use in such an investigation. Although a Gaussian form is a quite good representation of the α-particle density, somewhat more precise forms[76] could be incorporated relatively easily into the analysis. The nucleon-nucleon tensor interaction can give a small contribution[1,3] to $V_{\alpha\alpha}$ because of the presence of a small D-state admixture[77] in the α-particle wave function. The relatively minor, α-particle distortion (also termed polarization[1,3,78]) arising in the $\alpha + \alpha$ interaction can contribute to the long-range part of $V_{\alpha\alpha}$, and it would be desirable also to include this effect in the potential-model analysis.

APPENDIX: BEAM PROFILE CALCULATION

The beam model mentioned in Sec. III is that of Critchfield and Dodder[48] and was employed by Kan[49] to calculate the expression for the geometry factor G which we have used here. The model geometry which generates the beam is shown in Fig. 7 and consists of a source disk of radius d at a distance L from an aperture of radius c. The center of the scattering chamber is at a distance M from the aperture. The source disk is taken to
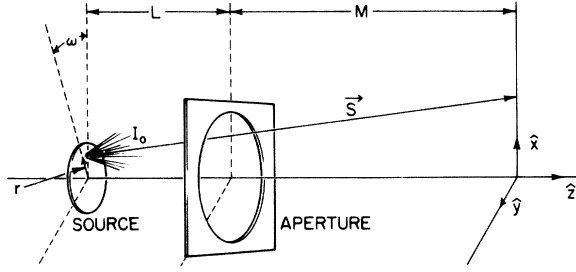
FIG. 7. Beam-model geometry. The source disk has radius d and the aperture has radius c. The origin of coordinates is at the center of the scattering chamber, and the y-z plane (for example) is the scattering plane.

produce a uniform time-integrated flux I_0 of particles per steradian per unit area of disk. The geometric parameters are to be chosen such that a realistic beam intensity distribution is obtained near the scattering-chamber center.

We calculate I, the number of particles passing through unit area of the plane $z = 0$ of Fig. 7. Because I is independent of the azimuthal angle about the z axis, we simply calculate it along the positive x axis:

$$I(x) = I_0 \int \vec{s} \cdot \hat{z} \; s^{-3} r \, dr \, d\omega . \tag{A1}$$

In Eq. (A1) the integration is over the area of the source disk which the aperture allows to be viewed from the point $(x, 0, 0)$, (r, ω) are polar coordinates specifying a particular point on the source disk, and $\vec{s}$ is the vector from the point (r, ω) on the disk to the point $(x, 0, 0)$. The aperture projection from point $(x, 0, 0)$ onto the plane of the source disk is a circle of radius r_0 with its center at the point $(-x_0, 0, -N)$, where

$$N = L + M, \quad r_0 = c N M^{-1}, \quad x_0 = x L M^{-1} . \tag{A2}$$

We treat x/N and r/N as small quantities and expand the integrand of Eq. (A1) to obtain

$$I(x) = 2 I_0 N^{-2} \int_{\omega_0(x)}^{\pi} d\omega \int_{r_1(\omega; x)}^{r_2(\omega; x)} Q(r, \omega; x) r \, dr , \tag{A3}$$

with

$$Q(r, \omega; x) = 1 - \tfrac{3}{2} N^{-2} (r^2 - 2xr \cos\omega + x^2) . \tag{A4}$$

The integration limits r_1, r_2, and ω_0 in Eq. (A3) have a variety of functional forms, which depend upon the relationships among the quantities x_0, r_0, and d. We will not list the forms for the limits here, but will simply give the final result for the beam intensity distribution $I(x)$. This is most easily accomplished by first defining several

quantities. Define I_g as

$$I_g = I_0 \sum_{n=1}^{4} g_n \sin(n\omega_1) , \tag{A5}$$

with

$$\cos\omega_1 = (r_0{}^2 - x_0{}^2 - d^2)/(2x_0 d), \quad g_1 = -2 x d^3 N^{-4} ,$$

$$g_2 = \tfrac{1}{2} x^2 L^2 N^{-2} M^{-2} (1 - 3c^2 N L^{-1} M^{-2})$$
$$\quad - \tfrac{3}{4} x^4 L^2 N^{-4} M^{-2} (1 + \tfrac{2}{3} L M^{-1}) , \tag{A6}$$

$$g_3 = 0, \quad g_4 = -\tfrac{1}{4} x^4 L^3 M^{-3} N^{-4} (1 + \tfrac{3}{4} L M^{-1});$$

define I_f as

$$I_f = \lambda I_0 \sum_{n=1}^{3} f_n \sin(n\omega_1) , \tag{A7}$$

with

$$\lambda = (1 - x_0{}^2 r_0{}^{-2} \sin^2\omega_1)^{1/2} = |r_0{}^2 + d^2 - x_0{}^2| / (2 d r_0),$$

$$f_1 = x c L M^{-2} N^{-1} (-1 + 2c^2 L^{-1} M^{-1} + \tfrac{9}{4} c^2 M^{-2})$$
$$\quad + \tfrac{3}{2} x^3 L c N^{-3} M^{-2} (1 + \tfrac{1}{2} L M^{-1}) ,$$

$$f_2 = 0, \quad f_3 = \tfrac{1}{2} x^3 c L^2 N^{-3} M^{-3} (1 + \tfrac{3}{4} L M^{-1}); \tag{A8}$$

and define I_1, I_4, I_2, and I_3 as

$$I_1 = I_0 \pi d^2 N^{-2} (1 - \tfrac{3}{4} d^2 N^{-2} - \tfrac{3}{2} x^2 N^{-2}) , \tag{A9}$$

$$I_4 = I_0 \pi c^2 M^{-2} (1 - \tfrac{3}{4} c^2 M^{-2} - \tfrac{3}{2} x^2 M^{-2}) , \tag{A10}$$

$$I_2 = I_1 \left(1 - \frac{\omega_1}{\pi}\right) + \frac{I_4}{\pi} [\omega_1 - \sin^{-1}(x_0 r_0{}^{-1} \sin\omega_1)]$$
$$\quad + I_g + I_f , \tag{A11}$$

and

$$I_3 = I_1 \left(1 - \frac{\omega_1}{\pi}\right) + \frac{I_4}{\pi} [-\pi + \omega_1 - \sin^{-1}(x_0 r_0{}^{-1} \sin\omega_1)]$$
$$\quad + I_g - I_f . \tag{A12}$$

The intensity $I(x)$, where $x \geq 0$, is given by the following tabulation:

Conditions	$I(x)$	Eq.
$r_0 \geq d + x_0$	I_1	(A9)
$r_0 \leq d + x_0, \; d \leq r_0 + x_0, \; x_0{}^2 \leq r_0{}^2 + d^2$	I_2	(A11)
$r_0 \leq d + x_0, \; d \leq r_0 + x_0, \; x_0{}^2 \geq r_0{}^2 + d^2$	I_3	(A12)
$d \geq r_0 + x_0$	I_4	(A10)
$x_0 \geq r_0 + d$	0	$\cdots$

Typical beam-model parameters, in mm, might be $d = \tfrac{1}{4}$, $c = \tfrac{3}{4}$, $L = 300$, and $M = 100$. These result in values of a few mm for D, the beam diameter at the scattering chamber center, and a few mrad for ϵ, the maximum angle which a particle in the beam can made with the z axis of Fig. 7. The quantities D and ϵ can be calculated from the formulas

$$D = 2(cN + dM)/L , \tag{A13}$$

and

$$\tan\hat{\epsilon} = (c + d)/L . \tag{A14}$$

*Work supported in part by the U. S. Atomic Energy Commission.

†Present address: Michigan State University, East Lansing, Michigan 48823.

[1]A. Herzenberg, Nucl. Phys. 3, 1 (1957).

[2]I. Shimodaya, R. Tamagaki, and H. Tanaka, Progr. Theor. Phys. 27, 793 (1962).

[3]S. Ali and A. R. Bodmer, Nucl. Phys. 80, 99 (1966).

[4]S. F. Edwards, Proc. Camb. Philos. Soc. 48, 652 (1952); J. Benn and G. Scharf, Helv. Phys. Acta 40, 271 (1967); P. B. Treacy, Nucl. Phys. A128, 241 (1969).

[5]O.Endo, I. Shimodaya, and J. Hiura, Progr. Theor. Phys. 31, 1157 (1964).

[6]V. G. Neudatchin, V. I. Kukulin, V. L. Korotkikh, and V. P. Korrenoy, Phys. Lett. 34B, 581 (1971).

[7]F. C. Barker, H. J. Hay, and P. B. Treacy, Aust. J. Phys. 21, 239 (1968).

[8]F. C. Barker, Aust. J. Phys. 22, 293 (1969).

[9]A. C. Butcher and J. M. McNamee, Proc. Phys. Soc. Lond. A74, 529 (1959); E. Van der Spuy, Nucl. Phys. 11, 615 (1959); E. W. Schmid and K. Wildermuth, ibid. 26, 463 (1961); S. Okai and S. C. Park, Phys. Rev. 145, 787 (1966); I. Reichstein and Y. C. Tang, Nucl. Phys. A139, 144 (1969).

[10]D. R. Thompson, I. Reichstein, W. McClure, and Y. C. Tang, Phys. Rev. 185, 1351 (1969).

[11]R. E. Brown and Y. C. Tang, Nucl. Phys. A170, 225 (1971).

[12]L. C. Neim, P. Heiss, and H. H. Hackenbroich, Z. Phys. 244, 346 (1971); private communication.

[13]F. E. Steigert and M. B. Sampson, Phys. Rev. 92, 660 (1953); J. L. Russell, Jr., G. C. Phillips, and C. W. Reich, ibid. 104, 135 (1956); R. Nilson, R. O. Kerman, G. R. Briggs, and W. Jentschke, Phys. Rev. 104, 1673 (1956); C. M. Jones, G. C. Phillips, and P. D. Miller, ibid. 117, 525 (1960); A. D. Bacher, F. G. Resmini, H. E. Conzett, R. de Swiniarski, H. Meiner, and J. Ernst, Phys. Rev. Lett. 29, 1331 (1972).

[14]D. J. Bredin, W. E. Burcham, D. Evans, W. M. Gibson, J. S. C. McKee, D. J. Prowse, J. Rotblat, and J. N. Snyder, Proc. Roy. Soc. Lond. 251, 143 (1959).

[15]R. Nilson, W. K. Jentschke, G. R. Briggs, R. O. Kerman, and J. N. Snyder, Phys. Rev. 109, 850 (1958).

[16]H. Werner and J. Zimmerer, in Proceedings of the International Conference on Nuclear Physics, Paris, 1964 (Editions du Centre National de la Recherche Scientifique, Paris, 1965), p. 241.

[17]T. A. Tombrello and L. S. Senhouse, Phys. Rev. 129, 2252 (1963).

[18]N. P. Heydenberg and G. M. Temmer, Phys. Rev. 104, 123 (1956).

[19]P. Darriulat, G. Igo, H. G. Pugh, and H. D. Holmgren, Phys. Rev. 137, B315 (1965).

[20]P. D. Curry and D. W. L. Sprung, Nucl. Phys. A216, 125 (1973).

[21]D. M. Brink and J. J. Castro, Nucl. Phys. A216, 109 (1973).

[22]G. F. Bertsch and W. Bertozzi, Nucl. Phys. A165, 199 (1971); R. M. Mendez-Moreno, M. Moreno, and T. H. Seligman, ibid. A221, 381 (1974).

[23]K. Wildermuth and W. McClure, in Springer Tracts in Modern Physics, edited by G. Hohler (Springer-Verlag, Berlin, 1960), Vol. 41.

[24]The property that exchange effects are of relatively short range is not a general feature of all systems. For example, see Figs 11 and 13 in Ref. 10 in which the $\alpha + \alpha$ and $n + \alpha$ systems are compared in this respect.

[25]C. H. Poppe, John H. Williams Laboratory of Nuclear Physics Annual Report, 1967 (unpublished), p. 141.

[26]R. E. Brown, J. A. Koepke, J. S. Lilley, and R. K. Snyder, John H. Williams Laboratory of Nuclear Physics Annual Report, 1974 (unpublished), p. 168.

[27]M. J. LeVine and P. D. Parker, Phys. Rev. 186, 1021 (1969).

[28]E. Huenges, H. Rösler, and H. Vonach, Phys. Lett. 46B, 361 (1973).

[29]Series 600, Ortec, Oak Ridge, Tenn. 37830.

[30]W. S. Chien, Ph.D. thesis, University of Minnesota, 1974 (unpublished).

[31]Taylor, Taylor and Hobson Ltd., Leicester, England.

[32]Model PTM-200, F. V. Fowler Co., Auburndale, Mass. 02166.

[33]Gage blocks, Fonda, Stamford, Conn.

[34]Research grade, Matheson Co., East Rutherford, N. J. 07073.

[35]Type-H polyimide film, Du Pont, Wilmington, Del. 19898.

[36]T. C. Kan, M.S. thesis, University of Minnesota, 1969 (unpublished).

[37]Co-rich alloy, Hamilton Watch Co., Lancaster, Pa. 17604.

[38]Type 170M, MKS Instruments, Burlington, Mass. 01803.

[39]Type FA-145, Wallace-Tiernan, Belleville, N. J. 07109.

[40]Type FA-135, Wallace-Tiernan, Belleville, N. J. 07109.

[41]Part No. 44032, Yellow Springs Instrument Co., Yellow Springs, Ohio 45387.

[42]Model 15-040A, Fisher Scientific Co., Pittsburgh, Pa. 15219.

[43]Model 1000, Brookhaven Instruments Corp., Brookhaven, N. Y. 11973.

[44]N. Jarmie, J. H. Jett, J. L. Detch, Jr., and R. L. Hutson, Phys. Rev. C 3, 10 (1971).

[45]The numerical coefficient in Eq. (1) was obtained by taking for e, the elementary charge, 1.602192×10^{-3} μC, for k, the Boltzmann constant, 1.380622×10^{-16} erg/K, and for the standard atmosphere 1.013250×10^{6} dyn/cm^2 = 760 Torr.

[46]The factor bP must be replaced by an appropriate average if target nuclei are present in more than one molecular species.

[47]E. A. Silverstein, Nucl. Instrum. Methods 4, 53 (1959).

[48]C. L. Critchfield and D. C. Dodder, Phys. Rev. 75, 419 (1949).

[49]J. T. C. Kan, Rev. Sci. Instrum. 44, 323 (1973).

[50]All quoted errors are standard deviations.

[51]A. S. Friedman, in American Institute of Physics Handbook, edited by D. E. Gray (McGraw-Hill, New York, 1963), 2nd ed., p. 4-158.

[52]E. D. Courant, Rev. Sci. Instrum. 22, 1003 (1951); E. J. Burge and D. A. Smith, ibid. 33, 1371 (1962); F. G. Resmini, A. D. Bacher, D. J. Clark, E. A. McClatchie, and R. de Swiniarski, Nucl. Instrum. Methods 74, 261 (1969).

[53]C. F. Williamson, J. P. Boujot, and J. Picard, Centre d'Etudes Nucléaires de Saclay Report No. CEA-R3042, 1966 (unpublished).

[54]F. D. Becchetti, Jr., private communication. The parameters of the optical potential were obtained from a preliminary global search on α+nucleus scattering data. The σ_R values given by these parameters agree to within 20% with computed and experimental values in J. R. Huizenga and G. Igo, Nucl. Phys. $\underline{29}$, 462 (1962); G. Igo and B. D. Wilkins, Phys. Rev. $\underline{131}$, 1251 (1963); L. McFadden, and G. R. Satchler, Nucl. Phys. $\underline{84}$, 177 (1966); A. Budzanowski, K. Grotowski, J. Kuzminski, H. Niewodiczanski, A. Strazalkowski, S. Sykutowski, J. Szmider, and R. Wolski, *ibid.* $\underline{A106}$, 21 (1968).

[55]We have also used this method to compute correction factors for p, d, and ^{3}He particles in silicon detectors and have compared these calculations with the experimental results of T. R. King, J. J. Kraushaar, R. A. Ristinen, R. Smythe, and D. M. Stupin, Nucl. Instrum. Methods $\underline{88}$, 17 (1970). We agree with their results for p, d, and ^{3}He particles, but for α particles we obtain a result 2.6 times smaller than they do. Because it is difficult to understand how either the dE/dx or σ_R values we used could be wrong by such a large factor, we believe the experimental result to be in error. Details of these comparisons are given in Ref. 30.

[56]Our experession for G_{00} is not the same as in Ref. 48 and our expression for Δ_0 has a term $(c^2+d^2)/(4L^2)$ replacing the term $-(c^2+d^2)/(2L^2)$ of Ref. 49. We have made these changes because the G_{00} of Ref. 49 implicitly contains terms of higher than second order in small quantities, even though such terms are not present in Δ_0, Δ_1, and Δ_2. This inconsistency in the formulas of Ref. 49 is of little practical importance, however.

[57]In evaluating χ^2, relativistic values have been used for the wave number k and the Coulomb parameter η. For comments on the importance of using a relativistic η value in low-energy $p+p$ analyses, see L. Durand, III, Phys. Rev. $\underline{108}$, 1597 (1957); M. de Wit and L. Durand, III, *ibid.* $\underline{111}$, 1597 (1958).

[58]R. A. Arndt and M. H. MacGregor, in *Methods in Computational Physics*, edited by B. Alder, S. Fernbach, and M. Rotenberg (Academic, New York, 1966), Vol. 6, p. 253.

[59]A. M. Lane and R. G. Thomas, Rev. Mod. Phys. $\underline{30}$, 257 (1958).

[60]In a single level fit, B may be given any value; its value simply effects the resultant E_λ, but nothing else.

[61]The fact that $-\phi_l$ need not be interpreted as purely a hard-sphere phase, but can be considered to contain contributions from other levels, is discussed in Sec. IV 1 c of Ref. 59.

[62]F. C. Barker, Aust. J. Phys. $\underline{25}$, 341 (1972).

[63]The presence of the $\alpha+\alpha$ * channel causes what is termed specific distortion in the $\alpha+\alpha$ channel. A detailed discussion of specific distortion in the $\alpha+\alpha$ system is given in D. R. Thompson, Y. C. Tang, and F. S. Chwieroth, Phys. Rev. C $\underline{10}$, 987 (1974).

[64]Discussions of the adjustment of u are given in I. Reichstein, D. R. Thompson, and Y. C. Tang, Phys. Rev. C $\underline{3}$, 2139 (1971); I. Reichstein and Y. C. Tang, Nucl. Phys. $\underline{A158}$, 529 (1970); and D. R. Thompson and Y. C. Tang, Phys. Rev. C $\underline{8}$, 1649 (1973).

[65]The determination of α, the α-particle size parameter, is described in Appendix A of J. A. Koepke, R. E. Brown, Y. C. Tang, and D. R. Thompson, Phys. Rev. C $\underline{9}$, 823 (1974).

[66]Such folded potentials are identical to direct potentials obtained with the resonating-group method.

[67]I. Reichstein and Y. C. Tang, Nucl. Phys. $\underline{A139}$, 144 (1969).

[68]R. A. Bryan and B. L. Scott, Phys. Rev. $\underline{135}$, B434 (1964); $\underline{164}$, 1215 (1967); $\underline{177}$, 1435 (1969).

[69]T. Ueda and A. E. S. Green, Phys. Rev. $\underline{174}$, 1304 (1968); Nucl. Phys. $\underline{B10}$, 289 (1969).

[70]S. D. Protopopescu, M. Alston-Garnjost, A. Barbaro-Galtieri, S. M. Flatté, J. H. Friedman, T. A. Lasinski, G. R. Lynch, M. S. Rabin, and F. T. Solmiz, Phys. Rev. D $\underline{7}$, 1279 (1973).

[71]M. M. Nagels, T. A. Rijken, and J. J. de Swart, Phys. Rev. Lett. $\underline{31}$, 569 (1973).

[72]These parameters are somewhat different from those given by the final analysis of Ref. 70; see footnote 6 of Ref. 71.

[73]The nonzero width of the isoscalar-scalar meson was included in the analysis of R. W. Stagat, F. Riewe, and A. E. S. Green, Phys. Rev. Lett. $\underline{24}$, 631 (1970).

[74]The narrow ω meson ($T=0$, $J^\pi=1^-$, $m_\omega c^2=784$ MeV, $\Gamma_\omega=10$ MeV, $g_\omega^2\approx10$) contributes a short-range repulsion to V_d; however, its effect is very small in the range $r>3$ fm.

[75]In the present work the repulsive components of $V_{\alpha\alpha}$ were given a Gaussian form. This form contains two parameters each, for $l=0$ and $l=2$. Recently, a form for the repulsive part of $V_{\alpha\alpha}$ has been used which contains only one parameter (a core cutoff radius) each, for $l=0$ and $l=2$. The strength of this repulsive part follows from arguments concerning the effect of the Pauli principle on the $\alpha+\alpha$ relative motion function [R. E. Brown, W. S. Chien, and Y. C. Tang, in Proceedings of the International Conference on Few Body Problems in Nuclear and Particle Physics, Quebec, 1974 (to be published)].

[76]R. F. Frosch, J. S. McCarthy, R. E. Rand, and M. R. Yearian, Phys. Rev. $\underline{160}$, 874 (1967).

[77]G. Abraham, L. Cohen, and A. S. Roberts, Proc. Phys. Soc. Lond. $\underline{A68}$, 265 (1955).

[78]S. D. Drell, Phys. Rev. $\underline{100}$, 97 (1955); A. Herzenberg and A. S. Roberts, Nucl. Phys. $\underline{3}$, 314 (1957).